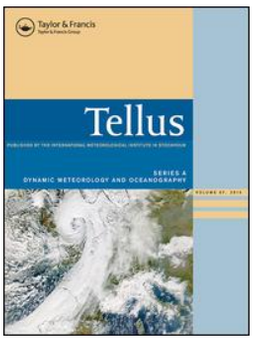

Tellus A: Dynamic Meteorology and Oceanography

ISSN: (Print) 1600-0870 (Online) Journal homepage: https://www.tandfonline.com/loi/zela20

Storm tracks and cyclone development using the theoretical concept of the Dynamic State Index (DSI)

Torsten Weber & Peter NÉevir

To cite this article: Torsten Weber & Peter NÉevir (2008) Storm tracks and cyclone development using the theoretical concept of the Dynamic State Index (DSI), Tellus A: Dynamic Meteorology and Oceanography, 60:1, 1-10, DOI: 10.1111/j.1600-0870.2007.00272.x

To link to this article: https://doi.org/10.1111/j.1600-0870.2007.00272.x

Tellus (2008), 60A, 1–10
Printed in Singapore. All rights reserved

TELLUS

Storm tracks and cyclone development using the theoretical concept of the Dynamic State Index (DSI)

By TORSTEN WEBER* and PETER NÉVIR, *Institut für Meteorologie, Freie Universität Berlin, Carl-Heinrich-Becker-Weg 6-10, 12165 Berlin, Germany*

(Manuscript received 6 March 2007; in final form 6 August 2007)

ABSTRACT

The Dynamic State Index (DSI) basing on the Energy-Vorticity Theory is able to detect all non-stationary and diabatic processes in the atmosphere. It is shown for the first time that the index is practicable for diagnostic analysis of the synoptic scale, in particular on pressure levels, using the ERA-40 reanalysis data set from the European Centre for Medium-Range Weather Forecasts (ECMWF). To verify the practical value of the DSI as a parameter diagnosing atmospheric developments, the index is applied to the synoptic scale. In a global view two different north hemispheric winters and particularly two case studies concerning the winter storm 'Lothar' and hurricane 'Andrew' are presented. For analysing the storm structures, both DSI on pressure levels and three-dimensional views of DSI isosurfaces are utilized. The results of this study document that the magnitude of the index expresses the intensification and decaying of the observed vortices. Thereby, it draws conclusions from the steering mechanism of 'Lothar' and 'Andrew' by virtue of their different DSI structures. A main result for practical weather forecasts is the early visibility of cyclones in the DSI field compared to the pressure field. Furthermore, storm tracks and their intensity can be visualized using the index.

1. Introduction

There is a number of diagnostic parameters for analysing structures of the atmosphere, which can be divided in the regarded scales. Ertel's potential vorticity (Ertel, 1942), Eady growth rate (Eady, 1949) or equivalent potential temperature are useful to analyse the large-scale conditions. Ertel's potential vorticity (PV) keeps material conserved in the absence of friction and diabatic processes. In the framework of modern PV-Thinking, the spatial distribution of this quantity can be used to estimate the atmospheric flow and temperature fields (Hoskins et al., 1985). On this account, it makes sense to observe the development of the PV during cyclogenesis phases. Wernli et al. (2002) show in their analysis of the winter storm 'Lothar' that a relationship exists between the intensification of the cyclone and two PV anomalies near its centre. The potential growth of extratropical cyclones is quantified by the Eady growth rate. This approach is applicable under the assumption that the zonal wind velocity does not change meridionally and the PV gradient is equal to zero. The last named parameter, the equivalent potential temperature, is utilized to specify different air masses. It indicates the temperature of an air parcel whose moisture was condensed out by a moist adiabatic process and the parcel brought dry-adiabatically down to 1000 hPa subsequently. Both parameters, the Eady growth rate and the equivalent potential temperature, were applied in the investigation of the three extreme winter storms in December 1999 by Ulbrich et al. (2001). To analyse the conditions on the convective scale, parameters like Level of Free Convection (LFC), Lifted Condensation Level (LCL) and Convective Available Potential Energy (CAPE) are used. Regarding the LFC, it is possible to estimate at which height an air parcel, lifted dry or moist adiabatically, becomes warmer than the surrounding air (e.g. McCoul and Cohen, 2002). The LCL describing the height at which an air parcel becomes saturated when it is lifted dry-adiabatically is applied in the works of Davies (2006) and Craven et al. (2002). Another variable quantifying the maximum energy of an air parcel which can be converted into kinetic energy during a possible ascent is called CAPE. López et al. (2001) found a correlation between increased CAPE values and the occurrence of thunderstorms and hailstorms on northwestern Spain. They came to the conclusion that CAPE should be used in combination with other parameters for hail forecasting.

All mentioned diagnostic parameters are derived from certain assumptions or specify only certain aspects of atmospheric processes. A novel Dynamic State Index (DSI) being a practical application of the Energy-Vorticity Theory (EVT) (Névir, 2004), detects all non-stationary and diabatic processes of the atmosphere and expresses them in terms of a single parameter. The innovative idea is to describe atmospheric developments relative

*Corresponding author. Max-Planck-Institut für Meteorologie, Bundesstrasse 53, 20146 Hamburg, Germany.
e-mail: torsten.weber@zmaw.de
DOI: 10.1111/j.1600-0870.2007.00272.x

to a well defined basic state. In the more stringent sense, the DSI marks the areas within the atmosphere deviating from this basic state, which can be considered as an energy-vorticity equilibrium. Consequently, the deviations are caused by non-stationary, diabatic processes and friction. A previous study of the DSI was restricted to investigate climatological questions and analysed the relationship between the index and precipitation (Névir and Brand, 2003). In this study, the index was calculated on isentropic levels whereas in this paper, the DSI is applied on the synoptic scale, in particular on pressure levels for the first time. Initially, in Section 2, the DSI is derived from the energy-vorticity coupling condition by two functional derivatives. In Section 3, a meteorological interpretation of the DSI and a relation between the index and general evolution of atmospheric processes are given. Section 4 briefly describes the data sets as well as the utilized methods for displaying the DSI. Subsequently, in Section 5, the index is calculated for two north hemispheric winters on the global scale. In Sections 6 and 7, selected development phases of the winter storm 'Lothar' and the hurricane 'Andrew' are analysed with the DSI. In this regard, the index on pressure levels and three-dimensional (3-D) views of DSI isosurfaces are used. Furthermore, the case studies contain a short synoptic overview of each extreme meteorological event. In Section 8, a summary of the results and an outlook close this investigation.

2. Dynamic State Index (DSI)

Changes in the atmospheric circulation are linked to synoptic activity, for example, growth of baroclinic waves and frontogenesis on the synoptic scale. These processes are coupled with ageostrophic non-balanced behaviour of unstable perturbances of atmospheric flow fields. The newly designed DSI is a measure for the deviation from the stationary solution of the adiabatic primitive equations and is a parameter to quantify these imbalances (Névir, 2004). The main result of the EVT for adiabatic non-viscous fluids is that two conserved quantities determine the non-linear evolution (Névir, 1998). The first globally conserved quantity is the total energy $\mathcal{H}$, given in the following form:

$$\mathcal{H} = \int_V \mathrm{d}\tau\rho \left[\frac{1}{2}\mathbf{v}^2 + \phi + e(v, s)\right]. \tag{1}$$

Hereby ρ denotes the density of the fluid, $\mathbf{v}$ the 3-D velocity, ϕ the potential of an external gravity field and $e = e(v, s)$ the specific internal energy as a function of the specific volume v and the specific entropy s. The second conserved global quantity is Ertel's potential enstrophy $\mathcal{E}_p$, which is a generalization of enstrophy for baroclinic fluids:

$$\mathcal{E}_p = \frac{1}{2}\int_V \mathrm{d}\tau\rho\Pi^2 \quad \text{with} \quad \Pi = \frac{\boldsymbol{\xi}_a \cdot \nabla s}{\rho}. \tag{2}$$

Here $\boldsymbol{\xi}_a = \boldsymbol{\xi} + 2\,\boldsymbol{\omega}$ is the absolute 3-D vorticity vector and $\boldsymbol{\omega}$ the angular velocity of the earth. Ertel's potential vorticity Π is a measure of the degree of rotational motion in an adiabatic 3-D fluid. Applying the EVT, a stationary solution can be derived for the whole set of the primitive equations if the total energy of the fluid is an arbitrary function of Ertel's potential enstrophy. Here, the most simple linear relationship is used:

$$\mathcal{H} = \lambda\,\mathcal{E}_p. \tag{3}$$

Constraint (3) is a global condition in terms of the two integrated conserved quantities. Moreover, this condition can be transformed to a constraint in terms of local fields by calculating the functional derivatives of the two quantities with respect to the density ρ and velocity $\mathbf{v}$ of the fluid. Thus, the functional derivatives are obtained:

$$\frac{\delta\mathcal{H}}{\delta\mathbf{v}} = \rho\mathbf{v}; \quad \frac{\delta\mathcal{H}}{\delta\rho} = B; \quad \frac{\delta\mathcal{E}_p}{\delta\mathbf{v}} = \nabla\Pi \times \nabla s; \quad \frac{\delta\mathcal{E}_p}{\delta\rho} = -\frac{1}{2}\Pi^2. \tag{4}$$

A comprehensive mathematical determination of the functional derivatives of Ertels potential enstrophy can be found in Appendix A. Combining the functional derivatives with eq. (3), the following equations result (Névir, 1993):

$$B = -\lambda\frac{1}{2}\Pi^2; \tag{5}$$

$$\rho\mathbf{v} = \lambda\nabla\Pi \times \nabla s. \tag{6}$$

Hereby denotes $B = 1/2\,\mathbf{v}^2 + \phi + e + pv$ the Bernoulli streamfunction. An equivalent expression for (6) was derived from PV and potential temperature without restriction to linear $\mathcal{H}$ and $\mathcal{E}$ by Blender (2005) introducing an additional time dependent χ-potential. Eliminating the constant λ by inserting the gradient of (5) in (6), the most general 3-D velocity representation is immediately obtained for a stationary adiabatic fluid without friction:

$$\mathbf{v} = \frac{1}{\rho\Pi}\nabla s \times \nabla B. \tag{7}$$

Using the whole set of primitive equations, Schär (1993) derived the same velocity representation in terms of the potential temperature θ:

$$\mathbf{v} = \frac{1}{\rho\Pi}\nabla\theta \times \nabla B \quad \text{with} \quad \Pi = \frac{\boldsymbol{\xi}_a \cdot \nabla\theta}{\rho}. \tag{8}$$

This 3-D solution describes a generalized energy-vorticity equilibrium, which is the most general stationary wind solution for the entire set of the primitive equations. On the basis of including all internal and external energy and vorticity quantities of the flow field, this general stationary wind is more realistic than the geostrophic or the pseudo-geostrophic wind approximation. Inserting (8) in the continuity equation for stationary flows $\nabla\cdot(\rho\mathbf{v}) = 0$, the following Jacobian determinant, which is equal to zero in a stationary adiabatic case without friction, can be obtained (Appendix B):

$$\frac{\partial(\Pi, \theta, B)}{\partial(x, y, z)} = 0. \tag{9}$$

This gives rise to the definition of the DSI that locally includes the information on the entropy, energy and potential vorticity:

$$\mathrm{DSI} := \frac{1}{\rho}\frac{\partial(\Pi, \theta, B)}{\partial(x, y, z)}. \tag{10}$$

Because of the functional dependence of the Bernoulli streamfunction and the PV in the stationary energy-vorticity basic state (5), the index in this state is exactly zero (DSI = 0).

3. Meteorological interpretation of the DSI

The condition (DSI = 0) was deduced from the assumption of a stationary adiabatic atmosphere. Under these constraints, the atmosphere is in a balanced energy-vorticity basic state and the general stationary wind (8) flows along the lines of intersection of the surfaces of the Bernoulli streamfunction and the potential temperature. In general, the real atmosphere is affected by non-stationary and diabatic processes such as radiation, friction and phase transitions of water. Thus, every deviation from the general stationary wind and accordingly from the stationary energy-vorticity equilibrium (DSI = 0) is caused by the last named processes. Calculations show that in the areas of the atmosphere which deviate from this state, typical dipole structures of the DSI occur. In line with the EVT this dipole behaviour can be regarded as an oscillation of the atmosphere about the stationary energy-vorticity equilibrium. Another more synoptic explanation of the dipole behaviour is enabled by analysing the wind field and the distribution of the squared PV. In the centre of the dipoles, it was found a maximum of squared PV situated between the positive and the negative areas. The wind field shows that the current flows into the maximum of squared PV in the positive areas and out of the maximum in the negative ones. Actually, under certain approximations the DSI is given by the advection of half squared PV. For reasons of brevity, it is abstained from a derivation and representation of the formulas. An elementary confirmation of this explanation can be obtained by regarding the unit of the DSI:

$$[\,\mathrm{DSI}\,] = \frac{\mathrm{K^2\,m^4}}{\mathrm{kg^2\,s^3}} = \frac{[\,\Pi^2\,]}{\mathrm{s}} \quad \text{with} \quad [\,\Pi\,] = \frac{\mathrm{K\,m^2}}{\mathrm{kg\,s}}. \tag{11}$$

Thus, the DSI is equal to the temporal variation of a vorticity-dynamic quantity. Therefore, the DSI can be construed as a measure of changes in the atmospheric system caused by non-stationary and diabatic processes.

To clarify the practical application as well as the relation between general atmospheric developments and corresponding DSI values (Fig. 1), we consider a geographic region with two different stable weather conditions (state 1 and state 2) in which the atmosphere is arranged in an energy-vorticity basic state. Although the index in each stable weather condition has a value of zero, the pertinent meteorological fields (such as temperature, pressure or humidity) can be different in their configurations. When the weather conditions change (from state 1 to state 2), the atmosphere leaves the energy-vorticity basic state and moves into a non-balanced energy-vorticity state for a short time. During this period weather activity occurs in the considered region. With this new general approach, the atmosphere as a whole (global) or particular regions (such as Europe) can be analysed. In this context, the DSI offers a new tool for visualization of storm tracks or for the investigation of single storms from their genesis over their maturation until their decay.

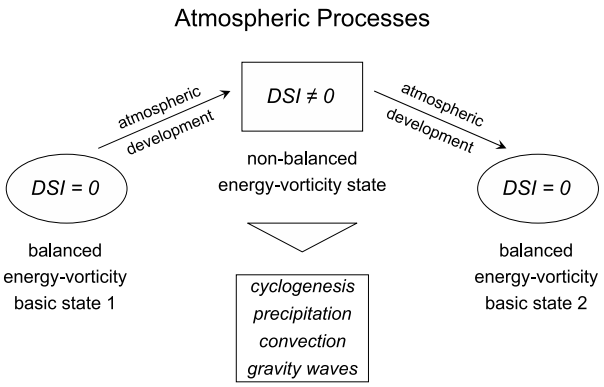

Fig 1. Relation between DSI and general atmospheric developments.

4. Data sets

In this study, data sets are used from the ERA-40 project. The provided ERA-40 data set supplied by the European Centre for Medium-Range Weather Forecasts (ECMWF) contains six-hourly reanalysis fields of several quantities on 14 pressure levels (1000, 925, 850, 775, 700, 600, 500, 400, 300, 250, 200, 150, 100 and 70 hPa) on a regular longitude/latitude grid with a horizontal resolution of 2.5°. For the calculation of the DSI, the following quantities must be available on pressure levels: Temperature, PV, geopotential height and the three components of the wind velocity. To display the DSI in a monthly mean, the index values are squared. This method avoids annihilating of the positive and negative values and allows a better scaling of the index. A particular property of the DSI values is their vertical variability up to three magnitudes in the troposphere. The minimum of the index values is found in 700–600 hPa and a maximum in the boundary layer as well as in the upper troposphere. This large variation is caused by various dynamic and diabatic processes prevailing in the different levels. For example, the minimum of the DSI values can be attributed to reduced non-balanced ageostrophic wind components. As a result of the vertical variability, it is necessary to normalize the DSI values in order to compare two different pressure levels. As a normalizing factor, the standard deviation of the DSI calculated on each pressure level and for one month using the six-hourly data is utilized (Table 1). In this way, it is also possible to compare different times within one month. The regions chosen for investigation are the North Atlantic Ocean including Europe and the Caribbean including the southwestern USA.

Table 1. Normalizing factors of the DSI used in the case studies

	Standard deviation	
	'Lothar' December 1999 75.0°N–35.0°N/ 12.5W–42.5°O	'Andrew' August 1992 40.0°N–10.0°N/ 100.0°W–30.0°W
Level [hPa]	$[10^{-18}\ K^2\ m^4\ kg^{-2}\ s^{-3}]$	$[10^{-18}\ K^2\ m^4\ kg^{-2}\ s^{-3}]$
100	904.6308	123.5209
150	486.8854	94.6343
200	380.1212	81.8446
250	318.4344	34.5175
300	170.6401	7.8548
400	61.5336	2.4135
500	15.4380	1.6399
600	7.7440	1.4532
700	7.0856	1.0709
775	8.2289	1.1058
850	10.9012	1.4203
925	18.4495	2.1266

5. Extra-tropical cyclones and storm tracks

In general, the largest atmospheric developments on the synoptic scale take place in the mid-latitudes, where strong cyclones with their appendant front systems are observed. Accordingly, in these zones, the DSI magnitude should be higher than in other regions. Two series of world maps of the squared DSI mean in the months December, January and February show different regions of high values in the mid-latitudes and northern polar regions (Figs. 2a–f). In December 1989 (Fig. 2a), a band of high index values extends from the westerly North Atlantic Ocean over Greenland Sea and Barents Sea to Siberia. This pattern can be interpreted as a cyclone track, which is shifted northward by a quasi-stationary anticyclone over central Europe. Moderate DSI magnitudes over the westerly Northern Pacific Ocean and in the Southern Hemisphere, in about 60°S, can be attributed to decreased cyclone activity.

In the following month (Fig. 2b), DSI values over the North Pacific and North Atlantic Ocean are much higher and cover larger areas that make up two southwest to northeast aligned bands. Moreover, a zone of moderate values can be observed over South Scandinavia and Russia. According to this, cyclone tracks over the North Pacific Ocean and the North Atlantic Ocean are more intensive and the quasi-stationary anticyclone over the European continent is weakened, so that the tracks are shifted southwards. Indeed, in the last third of January 1990, a period of stormy weather begun in Europe. The first one in a series of severe winter storms occurred at this time (McCallum, 1990) and two more, named 'Vivian' and 'Wiebke', crossed Europe

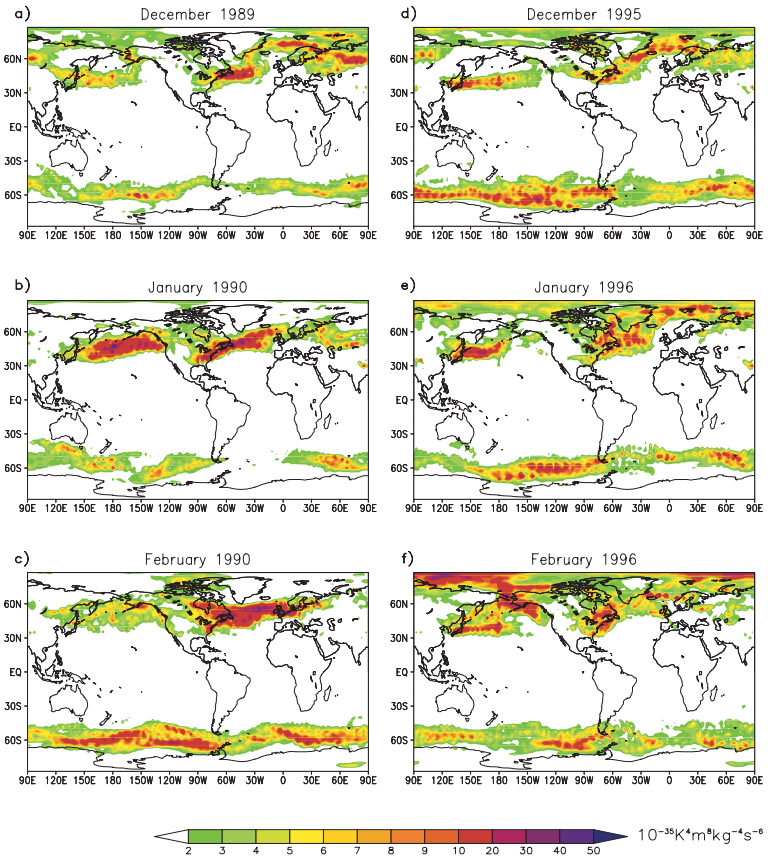

Fig 2. Monthly squared DSI mean in 500 hPa for two winters in the Northern Hemisphere. Displayed are (a)–(c) winter 1989/1990 and (d)–(f) winter 1995/1996. Coloured regions mark the cyclone and storm activity.

in February (Schüepp et al., 1994). The increased storm frequency over the continent is well displayed by a zone of high DSI magnitudes, which has extended to central Europe and northern Russia (Fig. 2c). In contrast to the situation in January, the cyclone activity over the North Pacific Ocean has decreased dramatically in February. At the same time, in the mid-latitudes of the Southern Hemisphere, high index values are detected indicating a strengthened cyclone activity.

A strong blocking weather condition over Europe can be found in the northern hemispheric winter 1995/1996. In December 1995 (Fig. 2d), cyclones take the same route as shown in December 1989, whereas over the westerly North Pacific Ocean, the cyclone activity is more intensive. Moreover, the mid-latitudes of the Southern Hemisphere are characterized by a strong westerly flow. One month later (Fig. 2e), Europe is completely devoid of cyclones caused by a more distinct stationary anticyclone. This weather condition led to a long-lasting cold and dry period in January 1996. At the same time, there is high cyclone activity over northeast Canada and the westerly North Atlantic Ocean as well as over the westerly North Pacific Ocean. The westerly flow in the Southern Hemisphere is less intensive compared to the month before and decays further in February (Fig. 2f). In the Northern Hemisphere, the main cyclone and storm activity occurs in the polar regions and over the North Pacific Ocean. Meanwhile, the blocking situation over Europe comes to an end. As a result, cyclones reach Great Britain and Scandinavia again.

6. Winter storm 'Lothar'

6.1. Description of the synoptic development

The cyclogenesis of 'Lothar' started off the East Coast of North America, at about 35°N, at 00 UTC 24 December 1999 (Fig. 3). There it formed a region of low depression (1017 hPa) in the south of a strong baroclinic zone with a meridional temperature gradient of more than 20 K over 700 km (Ulbrich et al., 2001). In the next 24 h, the cyclone relocated continuously, gradually dropping to 1000 hPa with more intensive precipitation to the northeast on the North Atlantic Ocean. During that period, 'Lothar' was on the southern side of the jet axis the entire time and was only present in the lower troposphere. The condition which led to quasi-stationary translation changed at 00 UTC 26 December when the cyclone headed for the European continent. At that time, 'Lothar' came under the influence of the delta of a jet stream lying in the approaches of the English Channel. Additionally, a PV anomaly emerged by infiltrating stratospheric air to the north of the vortex in the upper troposphere. At the same time, the production of PV increased as a result of released condensation heat in the lower troposphere (Wernli et al., 2002). The interaction of these two anomalies caused the rapid intensification of the vortex. At 06 UTC 26 December, the storm attained its maximum intensity over France with a central pressure of 961 hPa, wind gusts of almost 50 m s^{-1} and intensive precipitation. In the following 12 h, under slight attenuation, 'Lothar' moved across central Germany up towards the east–northeast where there were still wind gusts measured over 40 m s^{-1}. At 18 UTC on the same day, the decaying cyclone was located over southwestern Poland, about 500 km to the north of the jet axis, and both the PV anomaly in the upper and the anomaly in the lower troposphere had degenerated. Its central pressure had risen to 980 hPa and wind velocities and precipitation had further weakened.

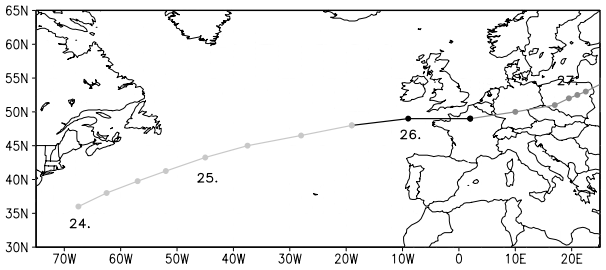

Fig 3. Map of 'Lothar's' track from 00 UTC 24 December 1999 to 12 UTC 27 December 1999. Dates indicate the position of the cyclone at 00 UTC of the current day and the temporal distance between two points is 6 h. Different development phases of 'Lothar' are marked by grey shadings: quasi-stationary translation (light grey), intensification (black) and weakening (dark grey).

6.2. DSI analysis of the severe winter storm

At first, the intensification phase of 'Lothar' is analysed in terms of horizontal DSI fields on pressure levels and vertical sections. Twelve hours before the winter storm reaches its maximum intensity, a clear dipole structure is visible at the position of 'Lothar'. On the contrary, there is almost no indication of cyclonic development in the 700 hPa pressure level (Fig. 4a). The vertical section shows that, at this time, the dipole extends from 850 to 600 hPa (Fig. 4b). Twelve hours later, the cyclone has developed into an intense vortex. This process leads to an amplification of the related dipole and the vertical DSI structure changed significantly (Fig. 5a and b). A second dipole appears in 300 hPh indicating an interaction between the upper and lower troposphere. Above all, a preceding trough is also characterized by two DSI dipoles over Eastern Europe in the vertical section. This seems to be a typical feature of mid-latitude cyclones generated by baroclinic instability.

In a second approach, 3-D structures of the DSI fields are displayed by isosurfaces −3/+3 (DSI normalized by standard deviation). This view affords the advantage of detecting the complete structure of the storm as compared to the DSI on single pressure levels. At 18 UTC 25 December 1999, a weak wave is detectable in the sea level pressure field (Fig. 6a). Above it, there is a characteristic dipole structure of the DSI in 700 hPa whereas no structure is yet observed in the upper troposphere. The expanded DSI structure over the European continent belongs to

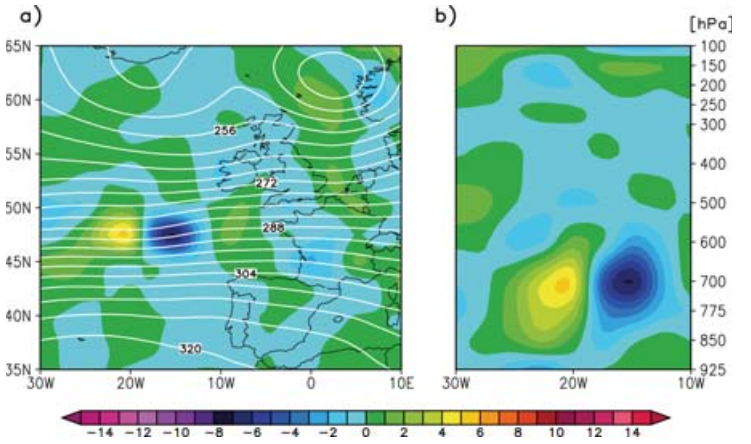

Fig 4. Twelve hours before 'Lothar' reaches its maximum intensity, a clear DSI dipole is detected at 18 UTC 25 December 1999: (a) DSI field and 700 hPa geopotential height (gpdm, white lines). (b) West–east oriented vertical section of the DSI field at 47.5°N from 30°W to 10°W (DSI normalized by standard deviation).

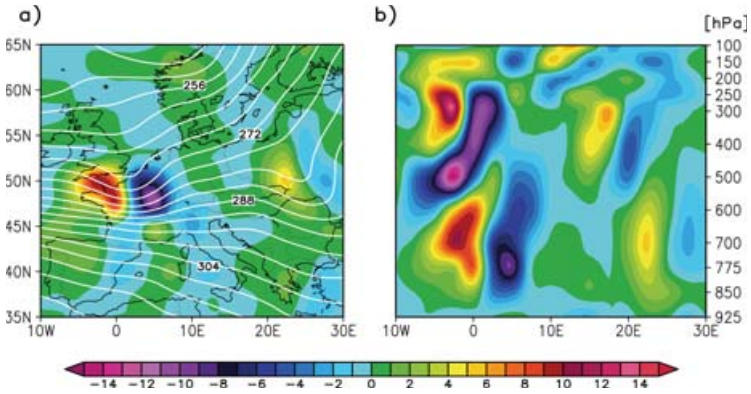

Fig 5. 'Lothar's' maximum intensity at 06 UTC 26 December 1999: (a) DSI field and 700 hPa geopotential height (gpdm, white lines). (b) West–east oriented vertical section of the DSI field at 50°N from 10°W to 30°E (DSI normalized by standard deviation).

a distinct cyclone over Scandinavia. Six hours later, at 00 UTC 26 December, the structure over the continent has separated into many small parts and the volume of the DSI dipole on the position of 'Lothar' has doubled (Fig. 6b). At the same time, an additional structure has been established in the upper troposphere. This pattern indicates that cyclogenesis also takes place in this region of the atmosphere. At 06 UTC 26 December, the time of maximum strength of the winter storm, the DSI isosurface in the upper troposphere widened downwards indicating the interaction of the upper and lower atmospheric flow field (Fig. 6c). The DSI structures during the intensification phase of 'Lothar' correspond very well with the results of a high-resolution model simulation of the 2 PVU isosurface (Wernli et al., 2002) at this time. Whereas this simulation indicates the PV isosurface, the DSI isosurface displays the deviation from the energy-vorticity equilibrium caused by non-stationary and diabatic processes. In the first approximation, this diagnostic approach is related to the temporal variability of the squared PV field.

7. Hurricane 'Andrew'

7.1. Life-cycle of a Category 5 hurricane

In the second half of August, 1992, Hurricane 'Andrew' developed from an easterly wave which moved westward across the North Atlantic Ocean. At 18 UTC 16 August, about 3000 km to the east of the Lesser Antilles, the wave reached the state of a tropical depression (Fig. 7). At that time, the clusters of showers associated with the wave, formed a closed cyclonic circulation. In the ensuing hours, deep convection intensified near the circulation centre and the maximum wind speed increased to 35 kn, so that, at 18 UTC 17 August, the National Hurricane Center (NHC) of the US National Oceanic and Atmospheric Administration (NOAA) classified the depression as a tropical storm. Afterwards, 'Andrew' moved along the southwestern side of a high pressure area situated over the eastern North Atlantic Ocean in 4 d. During that period, the central pressure dropped to 1000 hPa and then rose up to 1015 hPa whereas the maximum wind speed ranged between 35 and 45 kn. In the morning of 21 August, the storm turned west and headed for the Bahamas and the south of Florida where its central pressure started to fall and its wind speed rose up again.

As the storm formed an eye, the NHC upgraded the storm to a hurricane of Category 1 at 06 UTC 22 August. After 36 h more, 'Andrew' had grown stronger and the vortex was categorized as a hurricane of Category 5. At 18 UTC 23 August, a central pressure of 922 hPa and maximum wind speed of 150 kn were measured. In the night of 24 August, under slight attenuation, the hurricane moved across the Bahamas and the south of Florida where its wind speed of 145 kn and the accompanying storm surge of about

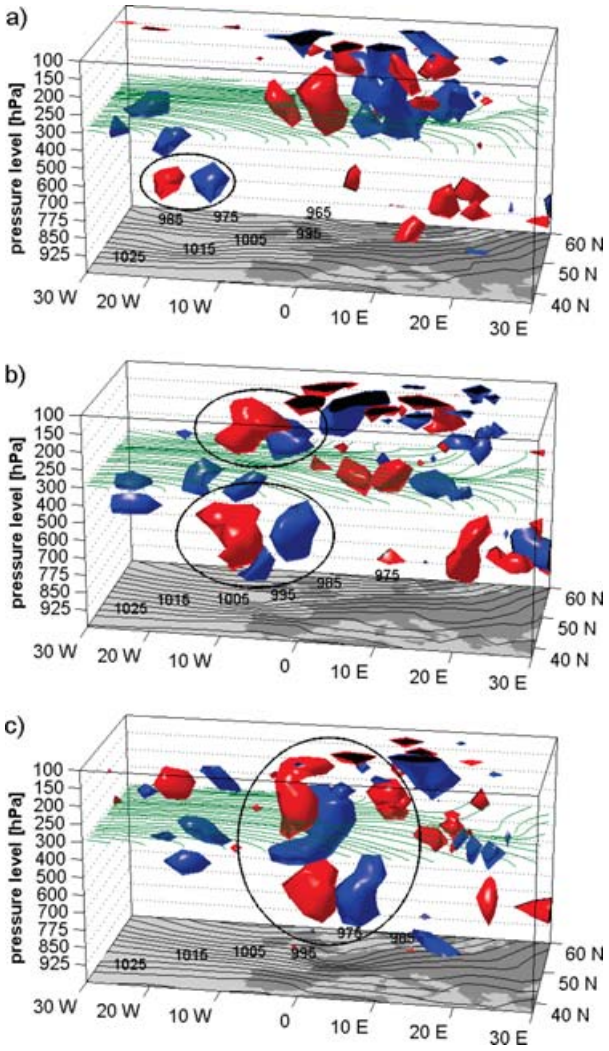

Fig 6. DSI isosurfaces −3/+3 (blue/red), streamlines (green) in 300 hPa and sea level pressure (hPa, black lines) during the intensification phase of 'Lothar' at (a) 18 UTC 25 December 1999, (b) 00 UTC 26 December 1999 and (c) 06 UTC 26 December 1999. Dipoles belonging to 'Lothar' are marked by circles.

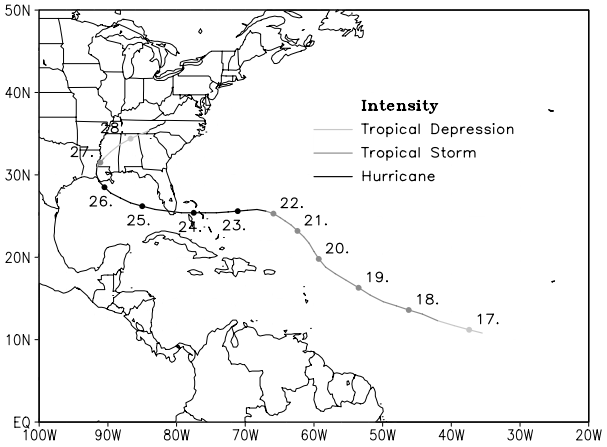

Fig 7. 'Andrew's' track from 18 UTC 16 August 1992 to 06 UTC 28 August 1992. Dates indicate the location of the cyclone centre at 00 UTC of the corresponding day.

4.5 m caused serious damage. After crossing Florida, 'Andrew' turned towards the north over the Gulf of Mexico and reached wind speeds of up to 100 kn and a central pressure of 956 hPa at the coast of Louisiana. Already at 18 UTC of 26 August, the hurricane had weakened so drastically that the NHC downgraded 'Andrew' to a tropical storm. Subsequently, on 28 August, the weakened storm changed its direction of movement to northeast and merged with a frontal system over southwestern USA. In association with 'Andrew' and its remnants, severe weather in the US Mid-Atlantic States was observed. The cyclone produced enough rainfall to cause local floods and several states even reported the occurrence of tornadoes which killed two people. For more detailed information see Landsea et al. (2004) and Rappaport (1994).

7.2. *DSI analysis of the tropical cyclone*

In contrast to the intensification phase of 'Lothar', the hurricane consists of only one dipole in the DSI field. A strong DSI signal arises when 'Andrew' is crossing the southern part of Florida at 12 UTC 24 August 1992 (Figs. 8a and 9a). At the position of the hurricane, a dipole structure exists between 400 and 600 hPa (Fig. 9b). The negative area of the dipole aligns in the direction of movement as seen in the case of the winter storm 'Lothar'. In addition, directly under the dipole structure the largest precipitation is detected. At this stage of development, the DSI detects the temporal evolution of the hurricane caused by non-stationary processes and phase transitions of water as well as marginal influence of friction. At 18 UTC 26 August, the dipole belonging to the hurricane is situated behind the coast line of Louisiana (Fig. 8b). 'Andrew's' landfall, 24 h later, and its subsequent unification with an extra tropical frontal system is also characterized by strong DSI signals which can be attributed to enhanced friction processes.

At 18 UTC 27 August, the volume of the DSI isosurface increased and widened downwards simultaneously as the precipitation under it became more intensive (Figs. 8c and 10a). The isosurfaces in the upper left corner of the picture (Fig. 8c) are affected by the frontal system, which starts merging with 'Andrew'. Thereby, at the position of 'Andrew's' remnants, the strongest DSI signals are located in the lower troposphere in about 700 hPa (Fig. 10b). Moreover, it seems that the upper part of the dipole starts separating, which may be interpreted as a transformation of the hurricane to an extra tropical cyclone. This DSI pattern resembles the observed structure of the storm 'Lothar' consisting of two separated dipoles. However, it must be

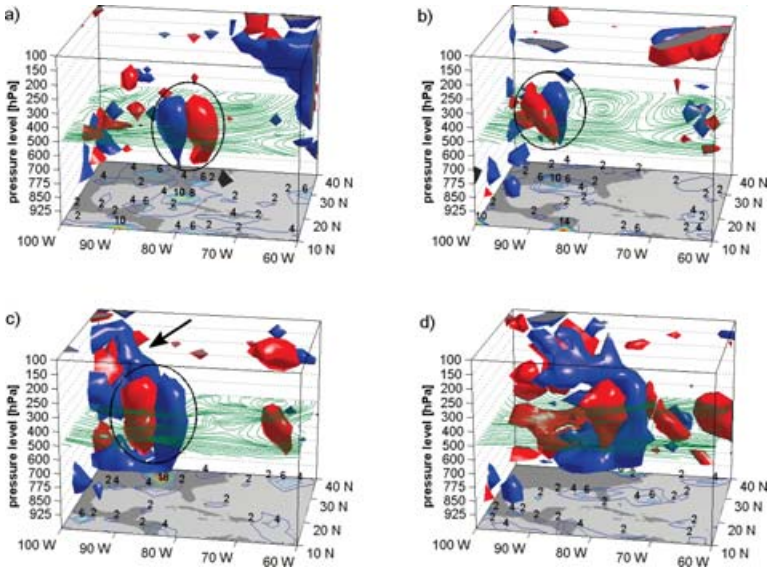

Fig 8. DSI isosurfaces −2/+2 (blue/red), streamlines (green) in 500 hPa and isolines of the accumulated precipitation up to the date (mm, coloured) at several development phases of 'Andrew'. (a) The hurricane is situated over the southern part of Florida at 12 UTC 24 August 1992. 'Andrew's' landfall and weakening at (b) 18 UTC 26 August 1992 and (c) 18 UTC 27 August 1992. (d) A frontal system and 'Andrew's' remnants merged at 18 UTC 28 August 1992. The dipole belonging to 'Andrew' is marked by a circle and the arrow points to an approaching frontal system.

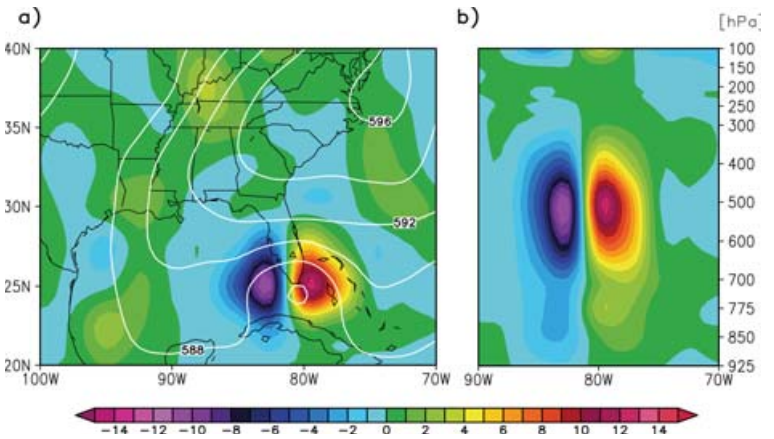

Fig 9. The hurricane is located over the top of Florida at 12 UTC 24 August 1992: (a) DSI field and 500 hPa geopotential height (gpdm, white lines). (b) West–east oriented vertical section of the DSI field at 25°N from 90°W to 70°W (DSI normalized by standard deviation).

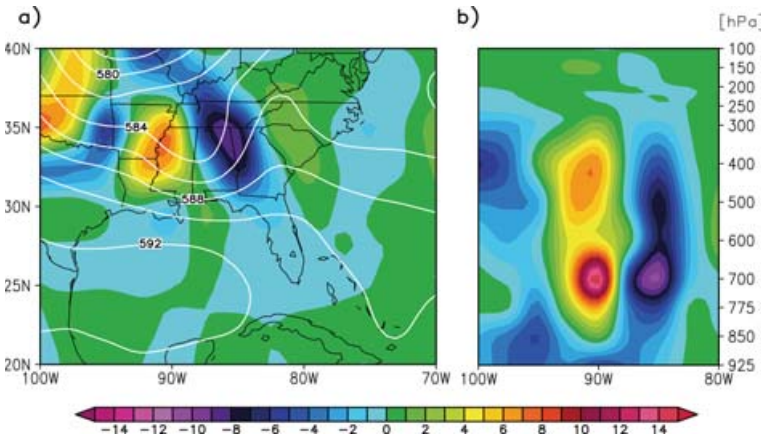

Fig 10. 'Andrew's remnants are situated over southwest USA at 18 UTC 27 August 1992: (a) DSI field and 500 hPa geopotential height (gpdm, white lines). (b) West–east oriented vertical section of the DSI field at 32.5°N from 100°W to 80°W (DSI normalized by standard deviation).

remarked that the weakening phase of 'Andrew' coincides with the unification of a frontal system. At 18 UTC 28 August, the DSI isosurfaces of the frontal system and the dipole of the hurricane, now downgraded to a tropical depression, merged (Fig. 8d). The DSI pattern and its strength in this period can be assigned to violent non-stationary and frictional processes as well as phase transitions of water which play a decisive role in the weakening phase. Generally, a time delay of about 18–24 h between the

significant DSI pattern and 'Andrew's' final landfall are observed (regarding the pressure and the wind speed). This can mark the timescale of the interaction between small scale processes in the boundary layer and mesoscale processes. Another explanation for the time delay may be the low spatial data resolution.

8. Summary and conclusion

The paper describes the first application of the DSI on the synoptic and planetary scale. In a global view two different north hemispheric winters and two case studies concerning the winter storm 'Lothar' and hurricane 'Andrew' are presented. In this investigation, the DSI is calculated on pressure levels using the ERA-40 reanalysis data set. As a main result, the squared index is able to identify the location and the strength of extra tropical storm tracks on pressure levels. Thereby, the storm tracks are detected as a deviation from an energy-vorticity basic state. Furthermore, the DSI is used to analyse the winter storm 'Lothar' and the hurricane 'Andrew'. These case studies prove that the DSI indicates the atmospheric development in extreme cyclones caused by non-stationary and diabatic processes. A comparison of the DSI structures of the winter storm and the hurricane shows fundamental differences. 'Lothar' consists of one dipole in the lower troposphere in its early phase and an additional one in the upper troposphere in its phase of intensification. On the contrary, 'Andrew' is characterized by only one dipole in the middle of the troposphere up to its unification with a frontal system.

A general result is the early visibility of both cyclones in the DSI field compared with the pressure field. Further, a maximum of squared PV in the centre of the DSI dipoles is observed and in both case studies, the negative areas of the dipoles are always oriented in their direction of movement. From a synoptic point of view, the current flowing into the maximum of squared PV in the positive areas and out of the maximum in the negative ones accounts for the dipoles. Another explanation of the dipole behaviour can be given in line with the EVT which regards the dipole occurrence as an oscillation of the atmosphere about the stationary energy-vorticity equilibrium. By means of the DSI, miscellaneous processes are uncovered which are responsible for the development and steering of both cyclones. In the case of 'Lothar', it is the interaction of diabatically produced squared PV in the lower troposphere with a predominantly and dynamically generated squared PV in the jet stream level. On the other hand, 'Andrew' is controlled by one maximum of this quantity which could be attributed to the release of latent heat and non-stationary flow conditions.

A further advantage of the DSI is its capability to detect cyclone activity in data sets with coarse gridpoint resolution. In the case of 'Lothar', a comparison of the analysis obtained by Wernli's high-resolution model simulation ($0.25^\circ \times 0.25^\circ$) and the resolution of the ERA-40 data set ($2.5^\circ \times 2.5^\circ$) shows up corresponding results. This motivates further investigation with higher data resolution. Moreover, it could be reasonable to compare the index with traditional methods such as band-pass filtering or Laplacian methods applied on maps of mean storm activity. Altogether, this study inaugurates the DSI analysis as a new diagnostic tool in dynamic meteorology.

9. Acknowledgments

The authors would like to thank the ECMWF for providing the ERA-40 data set and the two anonymous referees for giving helpful suggestions which led to several improvements of the manuscript.

10. Appendix A: Functional derivatives

In order to determine the functional derivatives of Ertels potential enstrophy with respect to the velocity and density, the following variation of $\mathcal{E}_p$ can be obtained:

$$\delta\mathcal{E}_p = \int_V \mathrm{d}\tau \left(\rho\Pi\,\delta\Pi + \frac{1}{2}\Pi^2\,\delta\rho \right). \tag{A1}$$

The variation of the PV as function of the velocity, the density and the specific entropy give

$$\begin{aligned}\delta\Pi &= \frac{\delta\boldsymbol{\xi}_a\cdot\nabla s}{\rho} + \frac{\boldsymbol{\xi}_a\cdot\nabla\delta s}{\rho} - \frac{\boldsymbol{\xi}_a\cdot\nabla s}{\rho^2}\delta\rho \\ &= \frac{\delta\boldsymbol{\xi}_a\cdot\nabla s}{\rho} + \frac{\boldsymbol{\xi}_a\cdot\nabla\delta s}{\rho} - \frac{\Pi}{\rho}\delta\rho.\end{aligned}$$

Inserting the variation of PV in (A1), the following equation results:

$$\delta\mathcal{E}_p = \int_V \mathrm{d}\tau \left(\Pi\,\delta\boldsymbol{\xi}_a\cdot\nabla s - \frac{1}{2}\Pi^2\delta\rho + \Pi\,\boldsymbol{\xi}_a\cdot\nabla\delta s \right). \tag{A2}$$

The first term in (A2) can be rewritten as

$$\Pi\,\delta\boldsymbol{\xi}_a\cdot\nabla s = \nabla\cdot(\Pi\,\delta\mathbf{v}\times\nabla s) + \delta\mathbf{v}\cdot(\nabla\Pi\times\nabla s)\,.$$

Inserting this expression in (A2), the theorem of Gauss can be applied to transform the first term in a closed surface integral assuming to vanish. This operation gives following result:

$$\delta\mathcal{E}_p = \int_V \mathrm{d}\tau \left[\delta\mathbf{v}\cdot(\nabla\Pi\times\nabla s) - \frac{1}{2}\Pi^2\delta\rho + \Pi\boldsymbol{\xi}_a\cdot\nabla\delta s \right]. \tag{A3}$$

From this equation the functional derivatives can be determined as

$$\frac{\delta\mathcal{E}_p}{\delta\mathbf{v}} = \nabla\Pi\times\nabla s\,; \quad \frac{\delta\mathcal{E}_p}{\delta\rho} = -\frac{1}{2}\Pi^2. \tag{A4}$$

Similar to this approach the functional derivative of the total energy with respect to the velocity and density can be obtained.

11. Appendix B: Jacobian determinant

The continuity equation for stationary flows is given by:

$$\nabla\cdot(\rho\mathbf{v}) = 0. \tag{B1}$$

Inserting the general stationary wind solution (8) in (B1), the following results are obtained:

$$\nabla \cdot \left[\frac{1}{\Pi} (\nabla\theta \times \nabla B) \right] = 0,$$

$$\frac{1}{\Pi} \nabla \cdot (\nabla\theta \times \nabla B) + \nabla \left(\frac{1}{\Pi} \right) \cdot (\nabla\theta \times \nabla B) = 0. \qquad \text{(B2)}$$

The first term of (B2) is equal to zero, because the curl of a gradient vanishes:

$$\nabla \cdot (\nabla\theta \times \nabla B) = \nabla B \cdot (\nabla \times \nabla\theta) - \nabla\theta \cdot (\nabla \times \nabla B) = 0.$$

Finally, the second term of (B2) can be written in the following way:

$$-\frac{1}{\Pi^2} \nabla\Pi \cdot (\nabla\theta \times \nabla B) = 0,$$

$$\nabla\Pi \cdot (\nabla\theta \times \nabla B) = \frac{\partial(\Pi, \theta, B)}{\partial(x, y, z)} = 0.$$

This shows that in case of stationary adiabatic flow conditions, the DSI is equal to zero.

References

Craven, J. P., Jewell, R. E. and Brooks, H. E. 2002. Comparison between observed convective cloud-base heights and lifting condensation level for two different lifted parcels. *Wea. Forecast.* **17**, 885–890.

Blender, R. 2005. Eulerian velocity reconstruction in ideal atmospheric dynamics using potential vorticity and potential temperature. *J. Phys. A: Math. Gen.* **38**, 6419–6428.

Davies, J. M. 2006. Tornadoes in environments with small helicity and/or high LCL heights. *Wea. Forecast.* **21**, 579–594.

Eady, E. T. 1949. Long waves and cyclone waves. *Tellus* **1**, 33–52.

Ertel, H. 1942. Ein neuer hydrodynamischer Wirbelsatz. *Meteorol. Zeitschrift* **59**, 277–281.

Hoskins, B. J., McIntyre, M. E. and Roberston, A. W. 1985. On the use and significance of isentropic potential vorticity maps. *Q. J. R. Meteorol. Soc.* **111**, 877–946.

Landsea, C. W., Franklin, J. L., McAdie, C. J., Beven II, J. L., Gross, J. M. and co-authors. 2004. A reanalysis of hurricane Andrew's intensity. *Bull. Amer. Met. Soc.* **85**, 1699–1712.

López, L., Marcos, J. L., Sánchez, J. L., Castro, A. and Fraile, R. 2001. CAPE values and hailstorms on northwestern Spain. *Atmos. Res.* **56**, 147–160.

McCallum, E. 1990. The Burns' Day storm, 25 January 1990. *Weather* **45**, 166–173.

McCoul, E. W. and Cohen, C. 2002. The impact on simulated storm structure and intensity of variations in the mixed layer and moist layer depths. *Mon. Wea. Rev.* **130**, 1722–1748.

Névir, P. 1993. Die Hamiltonsche Theorie der Hydrodynamik und ihre Anwendungen in der großräumigen Dynamik der Atmosphäre, Dissertation, Freie Universität Berlin.

Névir, P. 1998. Die Nambu-Felddarstellung der Hydro-Thermodynamik und ihre Bedeutung für die dynamische Meteorologie, Habilitationsschrift, Freie Universität Berlin.

Névir, P. 2004. Ertel's vorticity theorems, the particle relabelling symmetry and the energy-vorticity theory of fluid mechanics. *Meteorol. Zeitschrift* **13**, 485–498.

Névir, P. and Brand, S. 2003. Ein dynamischer Wetter- und Klima-Zustandsindex. *Terra Nostra, 6. Deutsche Klimatagung - Schriften der Alfred-Wegener-Stiftung*, 311–314.

Rappaport, E. N. 1994. Hurricane Andrew. *Weather* **49**, 51–61.

Schär, C. 1993. A generalization of Bernoulli's theorem. *J. Atmos. Sci.* **50**, 1437–1443.

Schüepp, M., Schiesser, H. H., Huntrieser, H., Scherrer, H. U. and Schmidtke, H. 1994. The winterstorm 'Vivian' of 27 February 1990: About the meteorological development, wind forces and damage situation in the forests of Switzerland. *Theor. Appl. Climatol.* **49**, 183–200.

Ulbrich, U., Fink, A. H., Klawa, M. and Pinto, J. G. 2001. Three extreme storms over Europe in December 1999. *Weather* **56**, 70–80.

Wernli, H., Dirren, S., Liniger, M. A. and Zillig, M. 2002. Dynamical aspects of the life cycle of the winter storm 'Lothar' (24–26 December 1999). *Q. J. R. Meteorol. Soc.* **128**, 405–429.